INTERNATIONAL JOURNAL FOR NUMERICAL METHODS IN FLUIDS
Int. J. Numer. Meth. Fluids 2009; **59**:91–115
Published online 28 April 2008 in Wiley InterScience (www.interscience.wiley.com). DOI: 10.1002/fld.1813

Incompressible SPH simulation of water entry of a free-falling object

Songdong Shao*, †, ‡

School of Engineering, Design and Technology, University of Bradford, West Yorkshire BD7 1DP, U.K.

SUMMARY

In this paper an incompressible smoothed particle hydrodynamics (Incom-SPH) model is used to simulate the interactions between the free surface flow and a moving object. Incom-SPH method is a two-step semi-implicit hydrodynamic formulation of the SPH algorithm and is capable of accurately treating the free surface deformations and impact forces during the solid–fluid interactions. For a free-falling object, its motion is tracked by an additional Lagrangian algorithm based on Newton's law to couple with the Incom-SPH program. The developed model is employed to investigate the water entry of a free-falling wedge. The accuracy of the computations is validated by the good agreement in predicting the relevant hydrokinematic and hydrodynamic parameters. Finally, a numerical test is performed to study the influence of spatial resolution on the water entry features. The Incom-SPH modeling coupled with the solid–fluid interaction algorithm could provide a promising computational tool to predict the slamming problems in coastal and offshore engineering. Copyright © 2008 John Wiley & Sons, Ltd.

Received 13 August 2007; Revised 7 January 2008; Accepted 25 February 2008

KEY WORDS: Incom-SPH; free surface; water entry; free-falling object; slamming force

INTRODUCTION

The study of water entry of a solid object has both theoretical and practical importance. The understanding of the complicated physical processes including the breakup of the free surface, solid–fluid interactions, turbulence and vortex generations, etc. is of great interest in fundamental environmental fluid mechanics. On the other hand, the water entry problem has also been a popular field of research in offshore and maritime engineering, e.g. in the diving of a submarine or the lowering of a marine vehicle. The knowledge of the flow field and slamming forces is necessary to make safety criteria during the designs and operations [1].

*Correspondence to: Songdong Shao, School of Engineering, Design and Technology, University of Bradford, West Yorkshire BD7 1DP, U.K.
†E-mail: s.shao@bradford.ac.uk
‡Lecturer in Environmental Fluid Mechanics.

Numerous experimental, theoretical and numerical studies have been performed to study the water entry problems. For example, Greenhow and Lin [2] conducted a series of experiments to show the considerable differences in the free surface deformation for the entry and exit of a circular cylinder. Zhao *et al.* [3] used both the experiment and the potential flow theory to investigate the water entry of a falling wedge. Similar water entry problems have also been studied by Tyvand and Miloh [4] using a series expansion approach and by Greenhow and Moyo [5] using a non-linear boundary element method model based on the irrotational flow assumption.

Numerical simulations based on the Navier–Stokes (N–S) equation have advantages in calculating the complicated interactions between the flow and an object. They are able to disclose very detailed information about the flow velocity field, impact pressure and slamming force, turbulence and vortex transport, etc. For example, Kleefsman *et al.* [6] and Panahi *et al.* [7] computed the water entry of a cylinder by solving the N–S equation with a volume-of-fluid surface tracking using a finite volume formulation. Meanwhile, an interactive fluid–body motion procedure derived from Newton's second law was coupled to their numerical schemes. More recently, Lin [1] used the concept of a locally relative stationary in his Reynolds-averaged N–S (RANS) modeling to study the water entry of a circular cylinder with prescribed falling velocity. In the model the solid motion is tracked using a Lagrangian method whereas the fluid motion around the solid body is solved using an Eulerian approach.

Particle modeling provides a robust numerical tool to simulate the complicated interactions between the flow and a solid body. Owing to the mesh-free nature, the breakup and reconnection of the free surfaces can be easily realized in a particle method without the sophisticated mesh management as required in a grid method. The capability of the particle model has been evidenced in the simulations of breaking wave impact on a moving float by Koshizuka *et al.* [8] and Gotoh and Sakai [9] using the moving particle semi-implicit (MPS) method. In this model, a simple-to-implement rigid-body tracking procedure was used to calculate the motion of a moving solid object. The smoothed particle hydrodynamics (SPH) method is another powerful particle modeling approach that uses highly accurate kernel functions to approximate the integrals. The SPH was originally developed for the astrophysical applications [10] and later adapted to the free surface flow simulations [11]. Oger *et al.* [12] employed the 2D SPH model with a fluid–solid coupling technique to study the water entry of a wedge with different degrees of freedom. The numerical model used a highly robust spatially varying particle resolution to improve the computational accuracy and efficiency.

In SPH models, an incompressible version of the SPH was invented by Shao and Lo [13], which has been recognized as an important step forward in the modeling of free surface flows. The incompressible SPH (Incom-SPH) approach differs from the original SPH [10] in that the pressure is calculated implicitly by a pressure Poisson equation, whereas in the original weakly compressible SPH the pressure was calculated explicitly by an equation of state derived from thermodynamics. The Incom-SPH model was shown to be able to realistically predict the pressure field of the flows due to its hydrodynamic formulations [14]. It has been applied to the wave overtopping [15] and the wave interactions with a floating curtain wall [16] in which the wave transmission features and impact forces were well reproduced by the model.

In this paper, the Incom-SPH model [13] will be coupled with a particle-based rigid-body tracking algorithm [8] derived from Newton's second law to study the water entry of a free-falling wedge. The calculations will be compared with the documented experimental and numerical data. The fundamental principles of the numerical model were originally developed by Shao and Gotoh [16] to simulate the wave interaction with a floating curtain wall, but here a new treatment procedure

DOI: 10.1002/fld

is applied to accurately satisfy the boundary conditions between the fluid and the falling wedge. A more robust particle link list based on the Verlet table is also used in the computations to improve the CPU efficiency. The numerical simulations aim at disclosing some important water entry features using the particle snapshots, velocity fields and impact pressures. Finally, the sensitivity of the model is analyzed by changing the spatial resolution of the particles and examining the computational results.

REVIEWS OF THE INCOM-SPH MODEL

In this section, the fundamental principles and formulations of the Incom-SPH model are reviewed.

Governing equations

The Lagrangian form of the N–S equation is solved in the Incom-SPH approach. In an SPH framework, the mass and momentum equations of the flows are represented as

$$\frac{1}{\rho}\frac{\mathrm{d}\rho}{\mathrm{d}t}+\nabla\cdot\mathbf{u}=0 \tag{1}$$

$$\frac{\mathrm{d}\mathbf{u}}{\mathrm{d}t}=-\frac{1}{\rho}\nabla P+\mathbf{g}+v_0\nabla^2\mathbf{u}+\frac{1}{\rho}\nabla\cdot\vec{\vec{\tau}} \tag{2}$$

where ρ is the density, t the time, $\mathbf{u}$ the velocity, P the pressure, $\mathbf{g}$ the gravitational acceleration, v_0 the laminar viscosity and $\vec{\vec{\tau}}$ the turbulent stress. Equations (1) and (2) are expressed in the form of a full derivative for the particle properties in order to implement the SPH formulations.

When dealing with the turbulent flows, the turbulent stress $\vec{\vec{\tau}}$ in Equation (2) needs to be modeled to close the equation. Here a large eddy simulation approach is used to model the turbulent stress as

$$\tau_{ij}/\rho=2v_{\mathrm{T}}S_{ij}-\tfrac{2}{3}k\delta_{ij} \tag{3}$$

where v_{T} is the turbulence eddy viscosity, S_{ij} the strain rate of the mean flow, k the turbulence kinetic energy and δ_{ij} the Kronecker delta. The turbulence eddy viscosity v_{T} is modeled by the simple and widely used Smagorinsky [17] model as

$$v_{\mathrm{T}}=(C_{\mathrm{s}}\Delta X)^2|S| \tag{4}$$

where C_{s} is the Smagorinsky constant (taken as 0.1 in this paper), ΔX the particle spacing, which represents the characteristic length scale of the small eddies and $|S|=(2S_{ij}S_{ij})^{1/2}$ is the local strain rate.

SPH formulations

The advantages of the SPH approach arise directly from its gridless nature. As there is no mesh distortion, the SPH method can effectively treat the large deformation of the free surfaces and interfaces between the fluid and solid in a pure Lagrangian way. In an SPH framework, the fluids are modeled as an assembly of individual particles and each particle is considered as a computational point. The motion of particles is calculated through the interactions with the neighboring particles by

DOI: 10.1002/fld

using an analytical kernel function. The governing equations are treated by the particle interaction models and thus the grid is not needed. For a detailed introduction of the SPH theory refer to Monaghan [10]. Among a variety of kernels documented in the literatures, the spline-based kernel normalized in 2D [10] is commonly used in the hydrodynamic calculations. The relevant SPH formulations used in this paper are summarized as follows.

The density of a fluid particle a is calculated by

$$\rho_a = \sum_b m_b W(|\mathbf{r}_a - \mathbf{r}_b|, h) \tag{5}$$

where a and b are the reference particle and its neighbors, m_b the particle mass, $\mathbf{r}_a$ and $\mathbf{r}_b$ are particle positions and W the interpolation kernel. Here h is called the smoothing distance or kernel length, which determines the range of particle interaction. A choice of h equal to $1.2\Delta X$ is usually made by balancing the computational efficiency and accuracy.

The pressure gradient uses a symmetric form as

$$\left(\frac{1}{\rho}\nabla P\right)_a = \sum_b m_b \left(\frac{P_a}{\rho_a^2} + \frac{P_b}{\rho_b^2}\right) \nabla_a W_{ab} \tag{6}$$

where the summation is over all the particles except particle a and $\nabla_a W_{ab}$ the gradient of the kernel taken with respect to the position of particle a. In a similar manner, the velocity divergence of a particle a is formulated by

$$\nabla \cdot \mathbf{u}_a = \rho_a \sum_b m_b \left(\frac{\mathbf{u}_a}{\rho_a^2} + \frac{\mathbf{u}_b}{\rho_b^2}\right) \cdot \nabla_a W_{ab} \tag{7}$$

The turbulent stress in Equation (2) can be formulated by applying the above SPH rule of divergence as

$$\left(\frac{1}{\rho}\nabla \cdot \vec{\vec{\boldsymbol{\tau}}}\right)_a = \sum_b m_b \left(\frac{\vec{\vec{\boldsymbol{\tau}}}_a}{\rho_a^2} + \frac{\vec{\vec{\boldsymbol{\tau}}}_b}{\rho_b^2}\right) \cdot \nabla_a W_{ab} \tag{8}$$

The second derivative of the laminar viscous force and the Laplacian of pressure are formulated by the hybrid of a standard SPH first derivative combined with a first-order finite difference approximation, following Cummins and Rudman [18] so as to avoid the numerical instability arising from particle disorders. They are expressed in a symmetric form as

$$(\nu_0 \nabla^2 \mathbf{u})_a = \sum_b m_b \frac{2(\nu_a + \nu_b)}{\rho_a + \rho_b} \frac{(\mathbf{u}_a - \mathbf{u}_b)(\mathbf{r}_a - \mathbf{r}_b) \cdot \nabla_a W_{ab}}{|\mathbf{r}_a - \mathbf{r}_b|^2} \tag{9}$$

$$\nabla \cdot \left(\frac{1}{\rho}\nabla P\right)_a = \sum_b m_b \frac{8}{(\rho_a + \rho_b)^2} \frac{(P_a - P_b)(\mathbf{r}_a - \mathbf{r}_b) \cdot \nabla_a W_{ab}}{|\mathbf{r}_a - \mathbf{r}_b|^2} \tag{10}$$

Incom-SPH solution process

In the Incom-SPH computation, the governing Equations (1) and (2) are solved using a two-step prediction and correction processes, as formulated by Shao and Lo [13] following Koshizuka *et al.* [8]. The prediction step is an explicit integration in time without enforcing the incompressibility, i.e. only the gravitational force, the turbulent and viscous forces in Equation (2) are used and

DOI: 10.1002/fld

an intermediate particle velocity and position are obtained. At this stage, the incompressibility or mass conservation of the fluid is not satisfied due to the particle motions, which is manifested by the deviation of the intermediate particle densities ρ_* from the initial values ρ_0. To re-enforce the incompressibility requirement, the pressure is used to update the intermediate particle velocity and position in the correction step.

The fluid pressure is computed from a pressure Poisson equation that is derived from combining the mass and momentum equations of (1) and (2), a process that is very similar to the projection method in a grid model. The pressure Poisson equation is formulated as [13]

$$\nabla \cdot \left(\frac{1}{\rho_*} \nabla P \right) = \frac{\rho_0 - \rho_*}{\rho_0 \Delta t^2} \tag{11}$$

It is noted that the source term on the right-hand side of Equation (11) is the difference in particle densities, whereas it is usually the divergence of intermediate velocity fields in an Eulerian grid model. This semi-implicit algorithm to calculate the fluid pressures distinguishes the Incom-SPH approach from the original weakly compressible SPH method [10] in which the pressure was explicitly calculated from an equation of state.

Flowchart of the Incom-SPH program

To provide a comprehensive view of the Incom-SPH solution procedures, a program flowchart is shown in Figure 1. For detailed mathematical formulations, refer to Shao and Lo [13] and Shao and Gotoh [16].

RIGID-BODY TRACKING ALGORITHM

To study the water entry of a free-falling object, additional procedures based on Newton's second law are needed to couple with the Incom-SPH model. Here the falling object is modeled by the particles with a fixed relative configuration and its motion is tracked by a passively moving solid model of Koshizuka *et al.* [8]. Firstly, the same computational procedures as stated in the previous section are applied to both the inner fluid particles and the solid body particles. In other words, the interconnections among the individual particles in the solid object are not considered at this stage and thus the solid body can deform. Secondly, an additional correction procedure is applied to the solid body particles only, to update their relative positions to the initial fixed configurations. If this correction procedure were not used, the solid object would behave similar to another fluid component with a different density.

Assuming that a solid object is composed of a number of particles each with a location at $\mathbf{r}_k$ and the number of the particles is n, the center of the solid object at $\mathbf{r}_c$, the relative coordinate of a solid particle to the center $\mathbf{q}_k$ and the moment of inertia I of the solid object are calculated by

$$\mathbf{r}_c = \frac{1}{n} \sum_{k=1}^{n} \mathbf{r}_k \tag{12}$$

$$\mathbf{q}_k = \mathbf{r}_k - \mathbf{r}_c \tag{13}$$

$$I = \sum_{k=1}^{n} |\mathbf{q}_k|^2 \tag{14}$$

DOI: 10.1002/fld

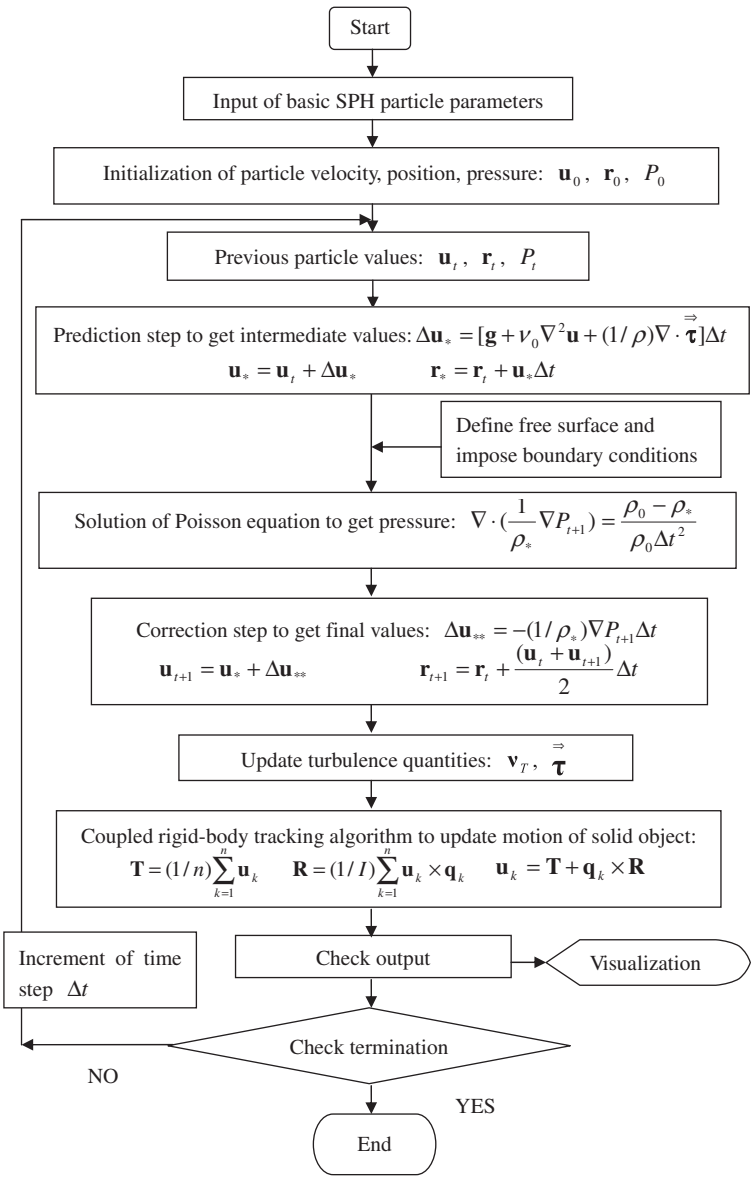

Figure 1. Flowchart of the Incom-SPH program.

The translational and rotational velocities of the solid object are calculated by

$$\mathbf{T} = \frac{1}{n}\sum_{k=1}^{n}\mathbf{u}_k \tag{15}$$

$$\mathbf{R} = \frac{1}{I}\sum_{k=1}^{n}\mathbf{u}_k\times\mathbf{q}_k \tag{16}$$

DOI: 10.1002/fld

Finally, the velocity of each particle in the solid body is updated to keep the original solid configuration by

$$\mathbf{u}_k = \mathbf{T} + \mathbf{q}_k \times \mathbf{R} \tag{17}$$

By applying the above rigid-body tracking corrections to the solid body particles, the motion of the free-moving object can be tracked as a complete rigid body. According to the latest study of Gotoh and Sakai [9], this simple procedure works very well in a stable computation where the Courant condition is satisfied, although the incompressibility may be temporarily violated. Refer to the program flowchart shown in Figure 1 for the numerical implementations.

TREATMENT OF FREE SURFACES AND BOUNDARY CONDITIONS

In this section, the numerical treatment procedures of the free surfaces, the fixed solid boundaries and the moving boundaries of the moving solid object are discussed.

Free surfaces

In the Incom-SPH computations, the free surfaces can be easily and accurately tracked by the fluid particles. As there is no fluid particle existing in the outer region of the free surface, the particle density on the surface should drop significantly. The criterion is that a particle can be judged as a free surface particle if its density is less than 1% of the inner fluid density, i.e. $990\,\mathrm{kg/m^3}$. To simplify the dynamic free surface boundary conditions, a zero pressure is given to each surface particle.

Fixed solid boundaries

The fixed solid boundaries such as the surrounding walls of the water tank are treated by fixed wall particles that balance the pressure of inner fluid particles and prevent them from penetrating the wall. The pressure Poisson equation (11) is solved on these wall particles using a homogeneous Neumann boundary condition. Several lines of dummy particles are placed outside of the solid wall to keep the fluid density at the wall particles consistent with that of the inner fluids. The velocities of both the wall and dummy particles are set at zero to represent a non-slip boundary. This computationally robust procedure was initially established by Koshizuka *et al.* [8] in the MPS method and was revised by Shao and Lo [13] in the Incom-SPH approach.

Moving solid boundaries

To study the detailed flow features near the moving solid boundaries of a free-falling object during the water entry, a mirror particle approach is used by following Colagrossi and Landrini [19] and Oger *et al.* [12].

In this approach, the fluid particles within a distance of $2h$ (kernel range) from the boundary of the moving solid object are mirrored across the boundary by following its local normal. The position of the mirror particles is set by a direct reflection of the corresponding inner fluid particles. The characteristics of the mirror particles, such as pressure, velocity, etc. are determined by using the properties of the corresponding inner particles. Let us assume that an inner fluid particle is i, with a pressure P_i and velocity $\mathbf{v}_i$, and its mirror particle is mi; the pressure relationship between

DOI: 10.1002/fld

them is

$$P_{\mathrm{mi}} = P_i \tag{18}$$

The relationship in velocity is

$$v_{\mathrm{mi}}^{\mathrm{n}} = (2\mathbf{v}_w - \mathbf{v}_i) \cdot \mathbf{n} \tag{19}$$

$$v_{\mathrm{mi}}^{\mathrm{t}} = \mathbf{v}_i \cdot \mathbf{t} \tag{20}$$

where $\mathbf{v}_w$ is the boundary displacement velocity of the moving solid, and $\mathbf{n}$ and $\mathbf{t}$ correspond to the normal and tangential directions of the solid boundary. Equations (19) and (20) describe non-penetration and free-slip boundary conditions, respectively. For an arbitrary-shaped boundary such as the wall of a circular cylinder, the mirroring should be performed by using the local tangential plane.

Implementations of fixed and moving solid boundaries

The use of mirror particles can result in a very accurate treatment of the solid boundaries, but at the cost of more CPU time. Therefore, in the Incom-SPH computations this procedure is only applied to the moving solid boundary of the falling wedge. For the side and bottom walls of the water tank they are simply treated by the fixed wall particles [8] to improve the computational efficiency. Besides, when applying the mirror particle approach, special attention should be paid to some singular points near the sharp edge where the mirroring of fluid particles may lead to excess particle mass. Appropriate corrections have to be made to avoid unrealistic mass accumulations as stated by Oger *et al.* [12].

PARTICLE LINK LIST WITH A VERLET TABLE

In the SPH computation, each particle requires a list of neighboring particles within a distance of the kernel range $2h$. The whole particle link list, which may be updated during each time step, requires the scale of N^2 operations in the calculation of the distances between all pairs of particles, where N is the total number of particles. This list generation can dominate the CPU time in a large simulation.

The block particle link list [13] has been widely used to identify the neighboring particles. In this process, a data structure is established to identify the neighboring particles within a distance of $2h$. The computational domain is divided into square cells each having a side length of $2h$ and a list of particles belonging to each cell is created. In the computation, a particle located within a given cell then considers the interactions only with the particles in the neighboring eight cells and the central cell.

In this paper a more robust particle link list based on the Verlet table has been used. The computational domain is still partitioned into square cells but this time with a side length being larger than the normal interaction range of $2h$. That is to say, the side length R is the sum of the interaction range $2h$ and a Verlet skin thickness ε. As the Courant condition is satisfied and the particle displacement is very small, we can generate a Verlet particle link list that does not need to be updated at every time step. Thus, the CPU efficiency can be greatly improved accordingly. Detailed descriptions of a Verlet table theory have been given in Oger *et al.* [12] and Viccione *et al.* [20].

DOI: 10.1002/fld

Different researchers have different interpretations of the optimum value of the thickness of the Verlet skin ε. For example, Oger *et al.* [12] suggested that the value of ε should be chosen so that in a Cartesian particle distribution, the neighboring numbers do not differ from the ones obtained in a radius equal to $2h$. Viccione *et al.* [20] made a detailed analysis on the optimum value of ε for different particle scales by simulating the run-up of a solitary wave. It was found that a Verlet skin of $0.6h$ could give the best performance in all the tests. This value will be adopted in the Incom-SPH simulations of a wedge entry in the following sections. We found that the CPU time was reduced by about 20% with the use of a Verlet table when compared with the use of a block particle link list only. To generate the neighboring particle list the Verlet table has also been successfully used to compute the breaking waves in the MPS method by Koshizuka *et al.* [8].

MODEL APPLICATIONS AND VERIFICATIONS

In this section, the Incom-SPH model coupled with a solid body tracking algorithm is used to simulate the water entry of a free-falling wedge, based on the experimental and numerical work of Zhao *et al.* [3], Kleefsman *et al.* [6] and Oger *et al.* [12]. The water entry features will be discussed through the particle snapshots, velocity fields and impact pressures. The computed falling velocity of the wedge and the slamming forces will be compared with the documented data.

Experimental setup

The experiment was carried out by Zhao *et al.* [3] at MARINTEK, Norwegian University of Science and Technology (http://books.nap.edu/openbook.php?record_id=5870&page=408). The drop test used a free-falling rig, which consists of the vertical guide rails, trolley, rotatable beam and test section. The test section was mounted on the beam. The total length of the test section is 1.0 m, the breadth is 0.5 m and the vertical distance from the keel to knuckles in the test section is 0.29 m. The V-shaped section has a 30° dead-rise angle and it is divided into a measuring section and two dummy sections on each side. The measuring section was connected to the drop rig using two force transducers. The total weight of the drop rig is 241 kg and a ballast weight of 100 kg is located within the beam. In the experiment, the vertical acceleration was measured using an accelerometer placed at the top of the test section and the vertical velocity was obtained using an optical sensor. The fluid forces were measured by the force transducers. The vertical motion is the only degree of freedom allowed to the wedge in the experiment. More details can be found in Zhao *et al.* [3], Kleefsman *et al.* [6] and Oger *et al.* [12].

Computational parameters

The numerical simulation is based on the above experiment to calculate the water entry of a free-falling wedge. As the velocity of the wedge during the entry process is not prescribed but depends on the interactions with the flow, the test could pose a big challenge to most grid models due to the treatment of free surfaces and moving solid boundaries. A 2D Incom-SPH computation has been made. The numerical water tank is 2 m wide and 1 m deep, and a particle spacing of $\Delta X = 0.01$ m was selected by balancing the computational efficiency and accuracy. In total, 20 000 particles are used in the simulations. The particles were initially placed in a Cartesian grid with the boundary particles constituting the boundary of the water tank and the edge of the falling wedge. The initial conditions were defined by using the exact velocity and position of the falling wedge at the impact

DOI: 10.1002/fld

moment in the experiment. The wedge entered the water surface with an initial falling velocity of 6.15 m/s. The laminar viscosity of the water is $\nu_0 = 10^{-6}\,\mathrm{m}^2/\mathrm{s}$ and the Smagorinsky constant is $C_s = 0.1$. The time step Δt was dynamically adjusted in the computations based on the Courant requirement.

Flow features during the wedge entry

From the SPH simulations, the computed particle snapshots during the wedge entry are shown in Figure 2(a)–(c). It shows that when the falling wedge touches on the water surface, the strong impact generates a large free surface deformation, with the water splash running out along the wedge boundary. The splashes direct upwards until they become unstable. At the initial stage of the impact, the water is pushed up but it attaches to the boundary of the wedge surface. As the wedge continues to move down, the water jet gradually detaches from the wedge boundary and plunges to the water surface. The Incom-SPH simulations of the flow features are similar to the experimental observations of Zhao *et al.* [3] and the numerical calculations of Kleefsman *et al.* [6] using a finite volume approach. The simulated flows are also similar to the computations of water entry of a circular cylinder by Lin [1] using a RANS model. The Incom-SPH model is able to disclose the complicated bending and splashing of the water jet. However, the calculated jet scale is smaller and weaker than that computed by Oger *et al.* [12] using a weakly compressible SPH approach. This could be attributed to the different particle spatial resolutions used in the two SPH runs. The Incom-SPH computation used a particle spacing $\Delta X = 0.01$ m, while a much more refined particle spacing $\Delta X = 0.001$ m was used in the impact areas by Oger *et al.* [12].

The computed velocity fields during the wedge entry are shown in Figure 3(a)–(c). The velocity fields were obtained by interpolating the individual particle velocity onto a 1 cm × 1 cm grid system in the computational domain using a standard SPH kernel. The figure shows that the entry of the falling wedge causes a drastic change in the velocity fields of the flow. The maximum jet velocity is about 10.0 m/s at $t = 0.004$ s and it increases to over 20.0 m/s at $t = 0.02$ s as the wedge further immerses into the water. The larger flow velocities and velocity variations concentrate in the water splash region and the interfaces between the flow and the wedge. Flow circulations can be sensed in these areas but they are not very clear presumably due to the relatively coarse spatial resolutions.

The computed pressure fields during the initial stage of wedge entry are shown in Figure 4(a) and (b), respectively, at time $t = 0.004$ and 0.016 s. From Figure 4(a), it is shown that a highly strong impact pressure is generated instantly at the moment of the falling wedge drops on the water surface. The maximum pressure value is about 100 kPa and it happens at the interface between the wedge boundary and the flow near the free surface. This large slamming force should be given great attention in practice, as it could damage the mechanical component of the structure and cause potential safety risks. However, as more parts of the wedge immerses into the water as shown in Figure 4(b), the maximum impact pressure reduces to 70% of the previous value and the trend is assumed to continue until the fluid force balances the gravitational force. The computed maximum pressure areas are generally consistent with the numerical results of Oger *et al.* [12], but the pressure distribution patterns of the two are different. The differences could be attributed to the different pressure solution methods in the two numerical models. In the Incom-SPH model, the pressure was implicitly calculated by a pressure Poisson equation, whereas the fluid pressure was explicitly solved by an equation of state in the weakly compressible SPH approach of Oger *et al.* [12]. Figure 4 also shows the advantages of the Incom-SPH formulation in that a reasonably stable pressure field can be obtained without artificial numerical smoothing. Besides, by examining the

DOI: 10.1002/fld

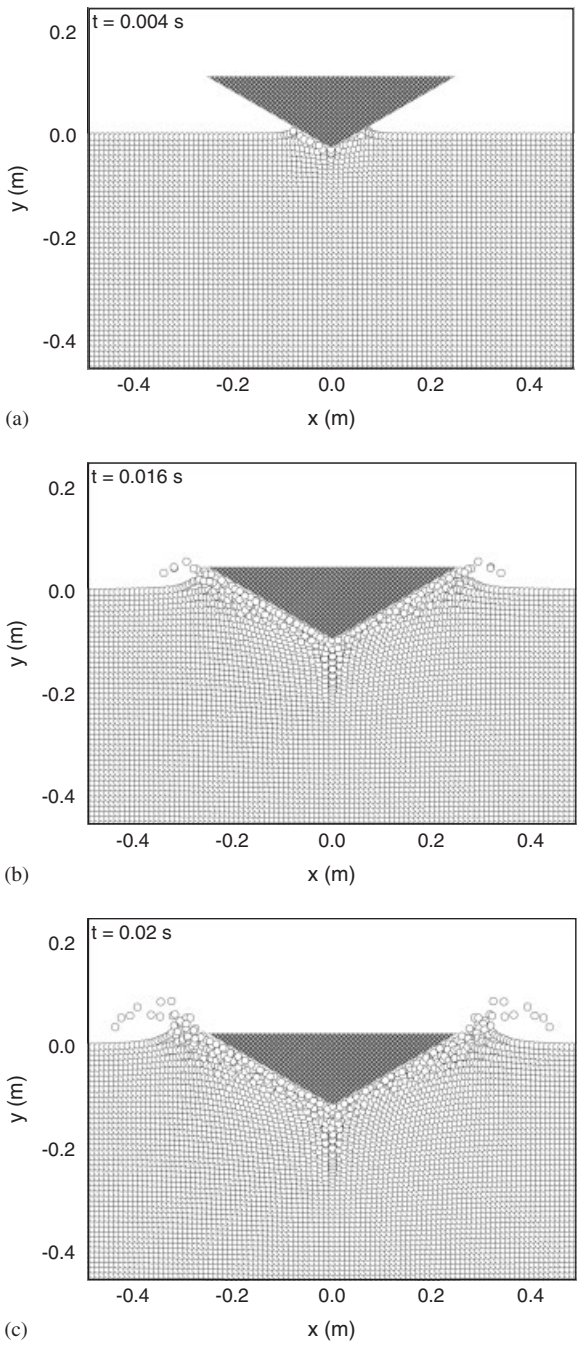

Figure 2. (a)–(c) Particle snapshots during wedge entry.

DOI: 10.1002/fld

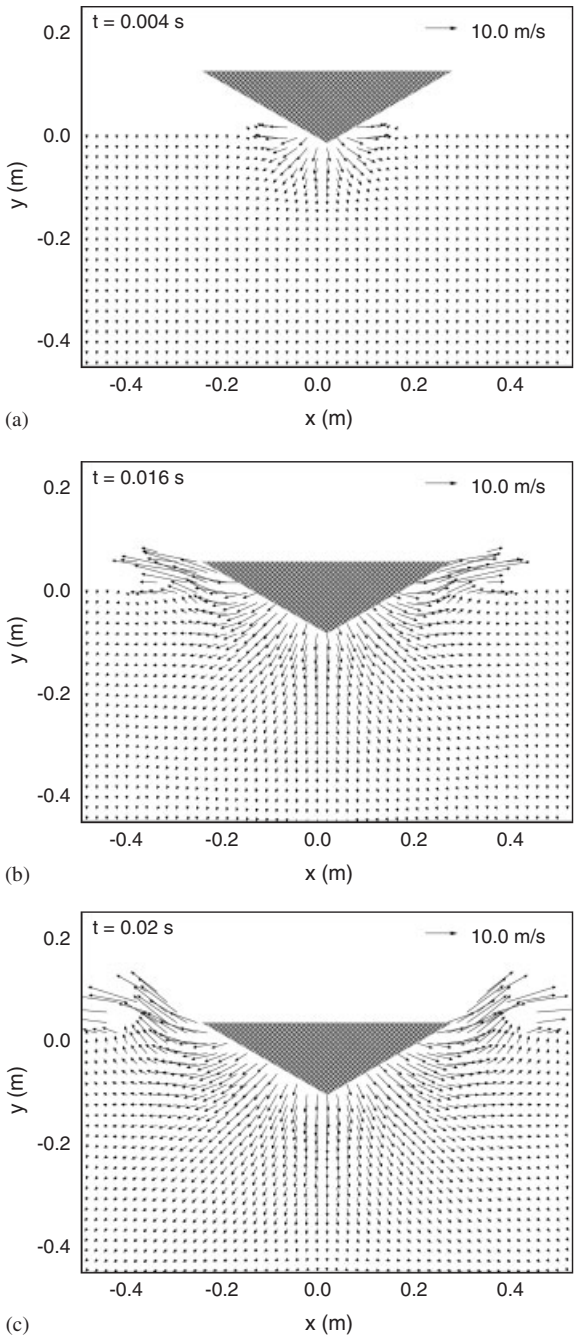

Figure 3. (a)–(c) Velocity fields during wedge entry.

DOI: 10.1002/fld

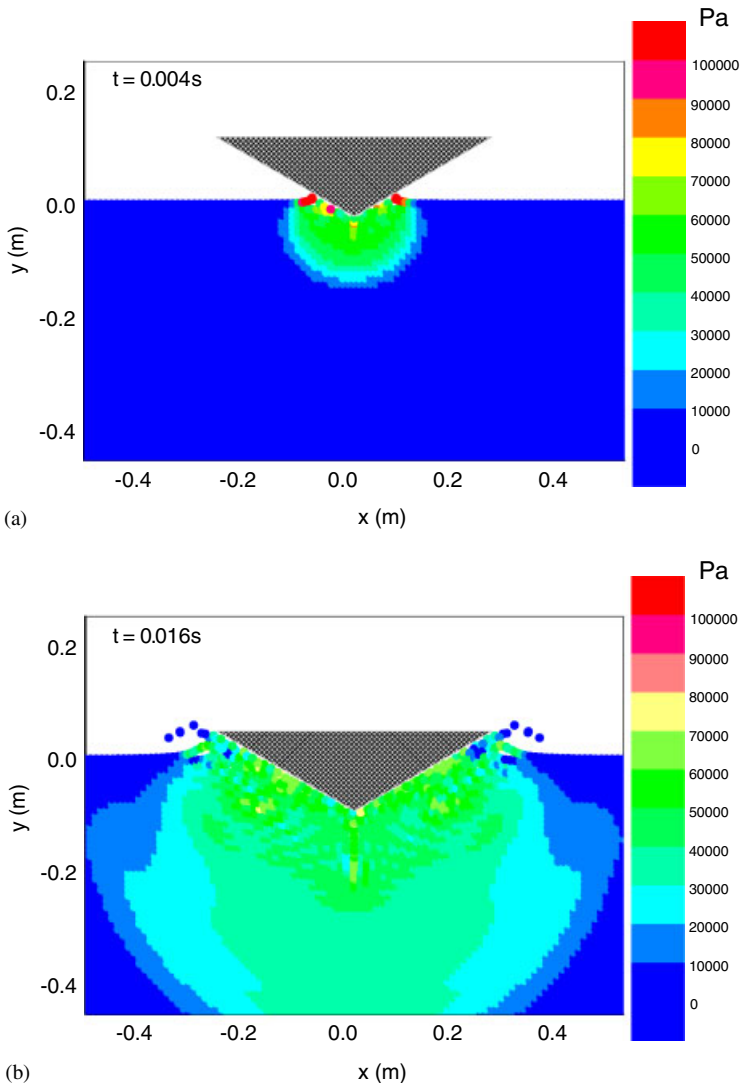

Figure 4. (a) and (b) Pressure fields during wedge entry.

pressure values of individual particles near the lower boundary of the water tank, it was found that the pressure disturbances can instantly spread to the particles far away from the impact region, which is due to the unlimited pressure wave speed in an incompressible fluid. However, this is not clearly reflected in Figure 4 and in Oger *et al.* [12] because the pressures in the impact region are the focus of interest in the figure illustrations.

Model verifications and result analysis

To quantitatively validate the accuracy of the Incom-SPH computations, the computed falling velocity of the wedge and the fluid forces acting on the wedge are shown in Figure 5(a) and (b),

DOI: 10.1002/fld

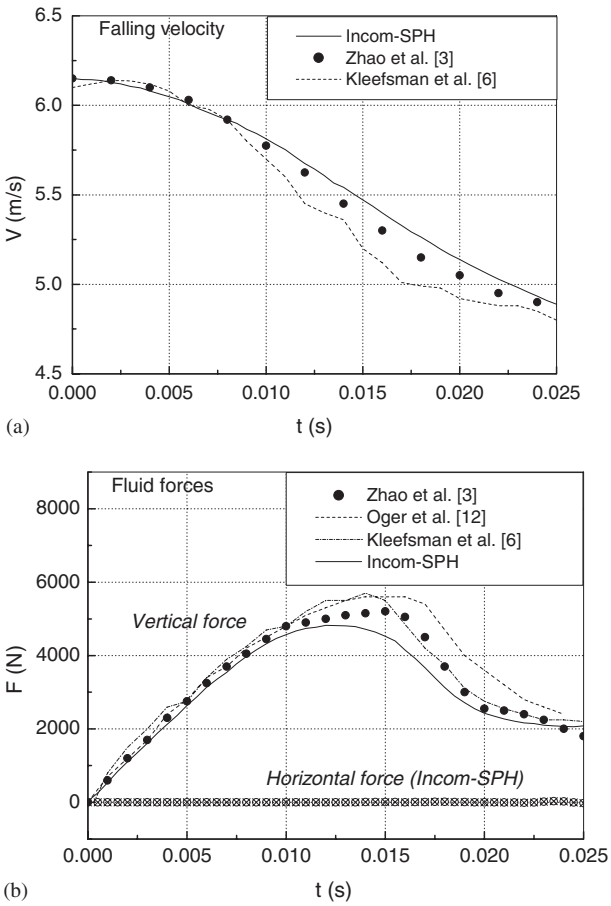

Figure 5. Time history of experimental and computed: (a) falling velocity and (b) fluid forces.

respectively. To make a comparison, also shown in the figure are the experimental data of Zhao *et al.* [3], the numerical results of Kleefsman *et al.* [6] by using a finite volume approach and Oger *et al.* [12] by using a weakly compressible SPH model.

It is shown from Figure 5(a) that the velocity of the falling wedge decreases a lot after it immerses into the water, because it is subjected to the hydrodynamic forces that result in a strong vertical deceleration to influence the motion of the wedge. The falling velocity computed by the Incom-SPH model agrees better with the experimental data [3] compared with the 3D finite volume calculations by Kleefsman *et al.* [6]. The maximum deviation between the numerical and experimental values is 2.2% in the Incom-SPH, whereas it is 3.1% in Kleefsman *et al.* [6].

The horizontal and vertical fluid forces acting on the falling wedge are shown in Figure 5(b), which was obtained by integrating the calculated pressures around the boundary of the wedge. The figure shows two different stages in the time history of the vertical fluid forces. In the first stage, the initial impact of the wedge on the water surface results in a drastic increase in the vertical slamming force until about time $t = 0.015$ s. In the second stage, as more and more parts of the wedge immerses into the water, the peak fluid force starts to decrease until time $t = 0.025$ s. In the

DOI: 10.1002/fld

figure, all the numerical results agree quite well with the experimental data of Zhao *et al.* [3] before $t=0.0125$ s. However, at time $t=0.015$ s, Kleefsman *et al.* [6] and Oger *et al.* [12] overpredict the peak fluid force by 5.8 and 7.7%, respectively, whereas the Incom-SPH computations underpredict the peak fluid force by 13.0%. After that, Kleefsman *et al.* [6] satisfactorily predicted the fluid force again, but Oger *et al.* [12] continued to overpredict it until $t=0.025$ s. On the other hand, the Incom-SPH computations continued to underpredict the experimental data until $t=0.018$ s but the agreement becomes better afterwards.

For the Incom-SPH computations, the overprediction of the falling velocity of the wedge in Figure 5(a) results from the underprediction of the vertical fluid forces in Figure 5(b). The disagreement with the experimental data [3] could be attributed to the 3D effect of the experimental conditions, inadequate spatial resolution in the computations and possible numerical errors. Kleefsman *et al.* [6] found that 3D computation with a coarser grid could get better results than 2D computation with a finer grid. From another point of view, we will use the numerical experiment to further study the influence of particle resolutions in the following section.

Finally, the computed horizontal fluid forces by the Incom-SPH model are also shown in Figure 5(b). It is shown that the horizontal forces remain nearly zero throughout the simulation process, which is consistent with the symmetric setup of the falling wedge. This could provide a self-check on the accuracy of the numerical formulations and solution algorithms in the Incom-SPH model.

SENSITIVITY ANALYSIS OF THE INCOM-SPH MODEL

The sensitivity of the numerical model is investigated by improving the spatial resolutions in the computations. To study the influence of particle spacing ΔX on the simulation results, the Incom-SPH model is rerun by using a finer particle spacing of $\Delta X=0.005$ m with other computational parameters being unchanged. The results are compared with the original computations in which a particle spacing of $\Delta X=0.01$ m was used.

The computed falling velocity of the wedge and the vertical fluid forces acting on the wedge are compared with the numerical results from the original SPH runs and the experimental data of Zhao *et al.* [3] in Figure 6(a) and (b), respectively. Although both Incom-SPH computations can predict the falling velocity and fluid forces in a good manner, the finer computations agree much better with the experiment. Especially, the finer computations accurately predict the peak fluid force at time $t=0.015$ s, which lead to a better agreement in the falling velocity.

The computed particle snapshots and velocity fields during the wedge entry by using $\Delta X=0.005$ m are shown in Figures 7 and 8(a)–(c), respectively. Compared with the original results in Figures 2 and 3(a)–(c), it is shown that more detailed flow features, such as the water surface breaking and the velocity structures near the wedge boundary, have been resolved by the finer particle size $\Delta X=0.005$ m. For example, the finer Incom-SPH computations in Figures 7(c) and 8(c) predict a much more violent splashing of the water jet. However, we should note that the simulated water splash-up is still weaker than that calculated by Oger *et al.* [12] using a particle size of $\Delta X=0.001$ m in the impact area. We did not attempt a higher particle resolution in the numerical test due to the constraint of CPU time that resulted from the use of a fixed kernel length in the Incom-SPH formulations.

The above comparisons between the original and refined Incom-SPH computations suggest that the influence of spatial resolutions or particle spacing is relatively small for the macroflow behaviors such as the falling velocity and fluid forces, but it is large for the refined structures of the water

DOI: 10.1002/fld

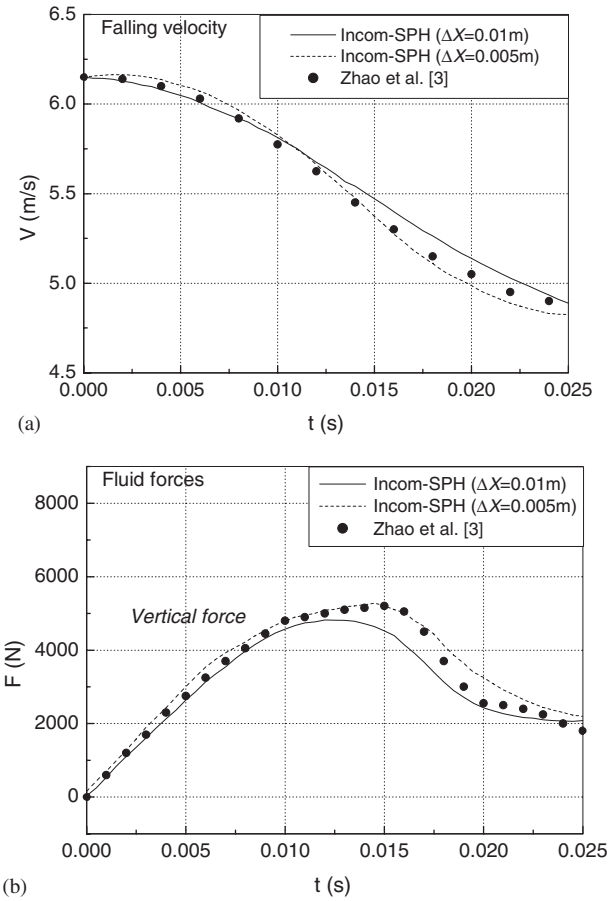

Figure 6. Time history of experimental and computed (using $\Delta X = 0.01$ and 0.005 m): (a) falling velocity and (b) fluid forces.

splash-up and velocity field. This is due to the fact that some detailed small-scale flows could be lost by using a coarser spatial resolution. Kleefsman *et al.* [6] drew similar conclusions by using three different grids in their finite volume computations. Besides, a sensitivity analysis on the turbulence modeling has also been carried out and the relevant details are presented in the Appendix.

CONCLUSIONS

A 2D Incom-SPH model has been developed to study the water entry of a free-falling object. The computations agree generally well with the documented experimental and numerical data by using a relatively coarse particle resolution, which shows that the model is capable of treating the large deformations of the free surface and the complicated interactions between the fluid and a solid. The disagreement with the data could be attributed to the 3D experimental conditions and inadequate particle resolutions. The Incom-SPH model has great potential to provide a promising

DOI: 10.1002/fld

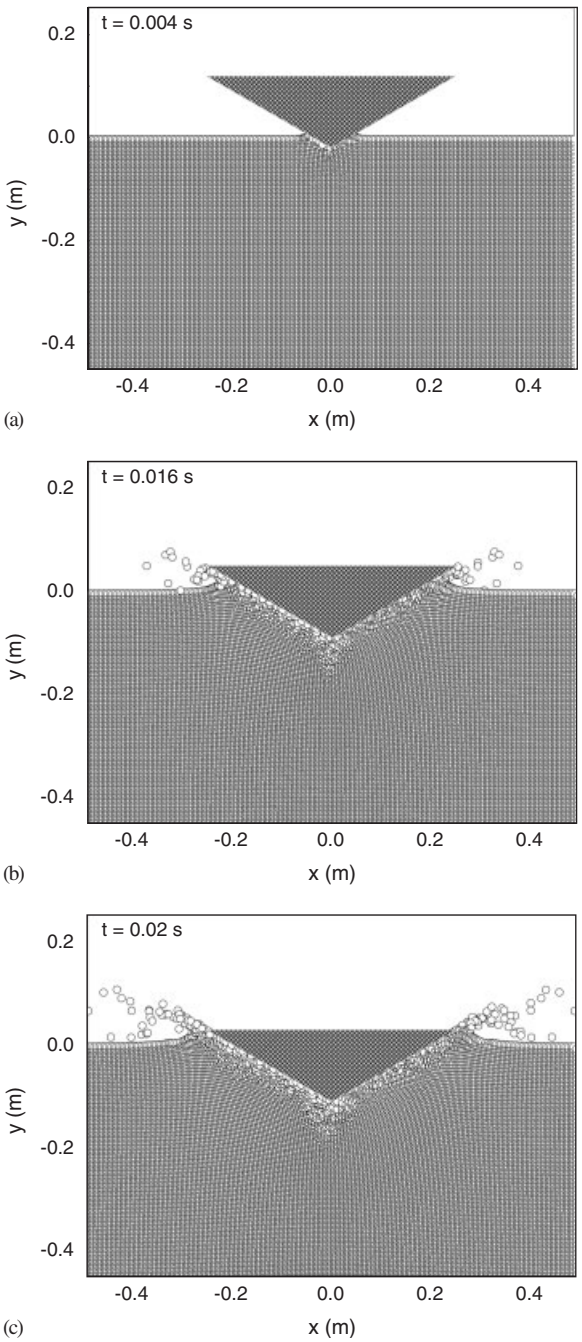

Figure 7. (a)–(c) Particle snapshots during wedge entry using $\Delta X = 0.005\,\mathrm{m}$.

DOI: 10.1002/fld

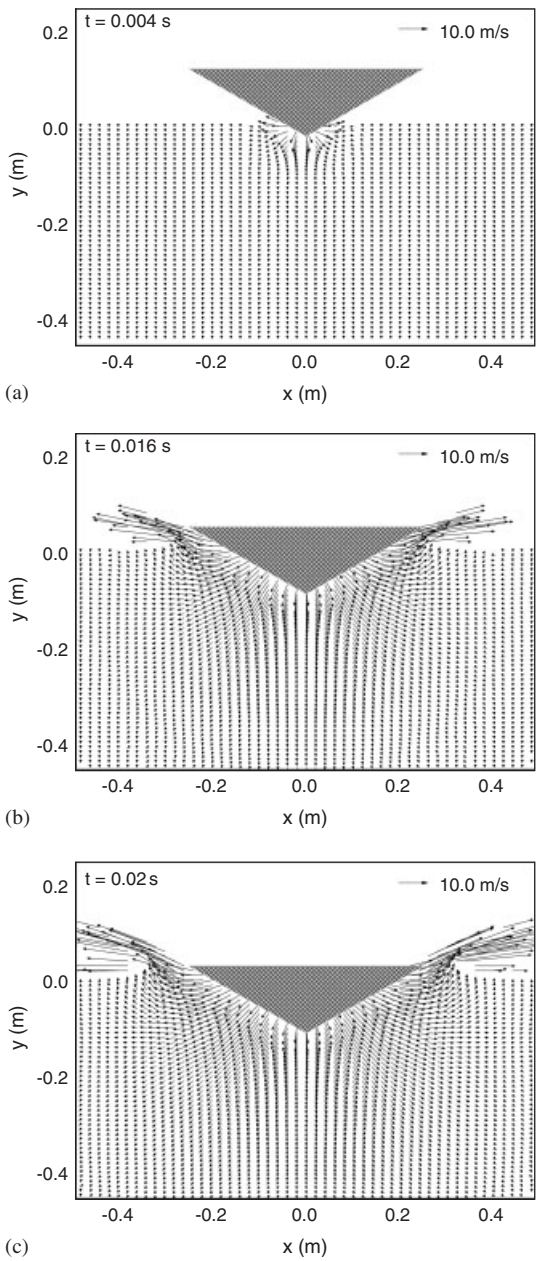

Figure 8. (a)–(c) Velocity fields during wedge entry using $\Delta X = 0.005\,\mathrm{m}$.

tool for a wide range of coastal and offshore applications, such as the structure responses to the flow action, the wave interactions with a floating body and the sinking of vessels in the open sea.

The sensitivity analysis of the numerical model has been carried out by refining the particle spacing ΔX. It is found that the spatial resolution can have a relatively large influence on the

DOI: 10.1002/fld

detailed flow structures in the water splash-up region, but it has less influence on the macroflow features such as the falling velocity of the object and the fluid forces. The finer the particle resolution is, the better the detailed flow structures can be resolved, but at the cost of more CPU time.

The Incom-SPH computations completed within a couple of hours using a CPU 2.13 G and RAM 1.0 G laptop. However, there is no CPU time available for a comparison in the literatures. It would be difficult to exactly evaluate the computational efficiency between the weakly compressible SPH of Oger *et al.* [12] and the Incom-SPH, as the sound wave speed limits the computational time step Δt in the former whereas the solution to pressure Poisson equation in the latter introduces the extra computational load. Here it is worth mentioning that Cummins and Rudman [18] compared the explicit and implicit SPH approaches and they found that the implicit SPH model has the potential to simulate incompressible flows more accurately and efficiently than the explicit model, especially as the Reynolds number is large.

In future work, a 3D Incom-SPH model will be developed to study the water entry problems in a more accurate manner.

APPENDIX A: TURBULENCE EFFECTS DURING WEDGE ENTRY

The study of turbulence generation and evolution at the moment of wedge entry is of great interest in practice. The computed turbulence eddy viscosity distributions (which is related to the turbulence kinetic energy) in the neighborhood of wedge surface at the initial stage of entry are shown in Figure A1(a)–(b), in which the viscosity values have been normalized by the laminar viscosity ν_0. It is shown that in the very beginning of the wedge entry at time $t=0.004$ s, the turbulence is generated very close to the wedge surface in a small region. The maximum eddy viscosity value is about 500 times of the laminar one. As the wedge continues to enter into the water until $t=0.016$ s, the influence of turbulence spreads into the inner flow region. The high turbulence area moves to the splash front and the maximum eddy viscosity value exceeds 1000 times of the laminar one. The figure indicates that the dominant turbulence influence (with the eddy viscosity value being larger than 500 times of the laminar one) is confined to a narrow region near the free surface in which the wedge surface and the flow are in contact.

To further study the influence of turbulence modeling on the water entry features of the falling wedge, the Incom-SPH model was rerun without the turbulence. This was achieved by deactivating the turbulence model and setting the Smagorinsky constant to $C_s=0.0$. Thus, only the laminar viscous force is considered in the computations rather than the turbulent shear force in the original run. The computed particle snapshots and velocity fields of the flow during the wedge entry are shown in Figures A2(a)–(c) and A3(a)–(c), respectively. Compared with the numerical results in Figures 2(a)–(c) and 3(a)–(c) obtained with the turbulence modeling, there exist some differences in the water surface breaking and jet formation. At time $t=0.016$ and 0.02 s, the computations without the turbulence model produce a relatively stronger water splash and the jet velocity was found to be 5% larger. It can be reasoned that the turbulence effect dampened the flow energy during the wedge entry, leading to a smaller and weaker water splash in the original runs.

Finally, detailed comparisons are made between the turbulence and non-turbulence runs for the falling velocity of the wedge and the fluid forces in Figure A4(a)–(b), in which the experimental data of Zhao *et al.* [3] are also shown. The figure indicates that the two numerical results agree reasonably well with the experimental data and they are quite close to each other except that the

DOI: 10.1002/fld

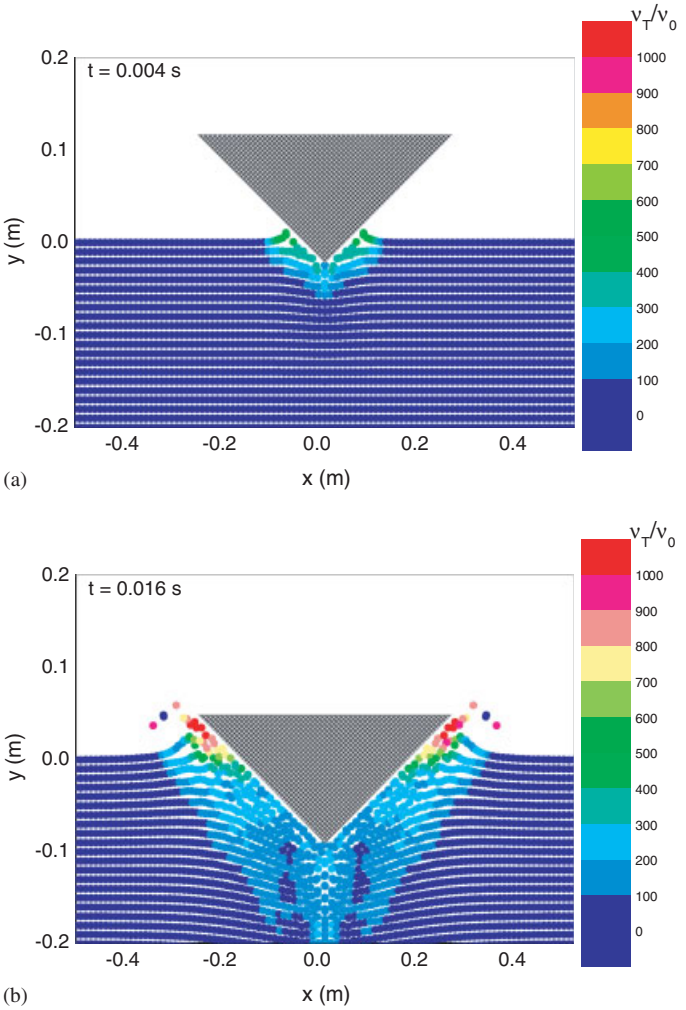

Figure A1. (a) and (b) Turbulence eddy viscosity distributions near wedge surface.

peak fluid force is overestimated by about 15% in the non-turbulence computations. This might suggest that without the adequate numerical dissipations from the turbulence generation, stronger particle interactions and collisions occurred and caused a relatively larger hydrodynamic force in the non-turbulence computations. However, the falling velocity of the wedge is almost unaffected due to the transient duration of the excessive fluid forces.

From the above analysis, it was found that the influence of turbulence modeling is mainly upon the detailed flow features near the water splash region, whereas the macroflow behaviors such as the falling velocity of the wedge and the fluid forces are not sensitive to this issue. Therefore, we could conclude that the turbulence effect is not an influential factor to be considered in similar wedge entry problems and a non-turbulence computation should be able to disclose most useful information we are interested in. Lin [1] also drew this conclusion based on the RANS simulations

DOI: 10.1002/fld

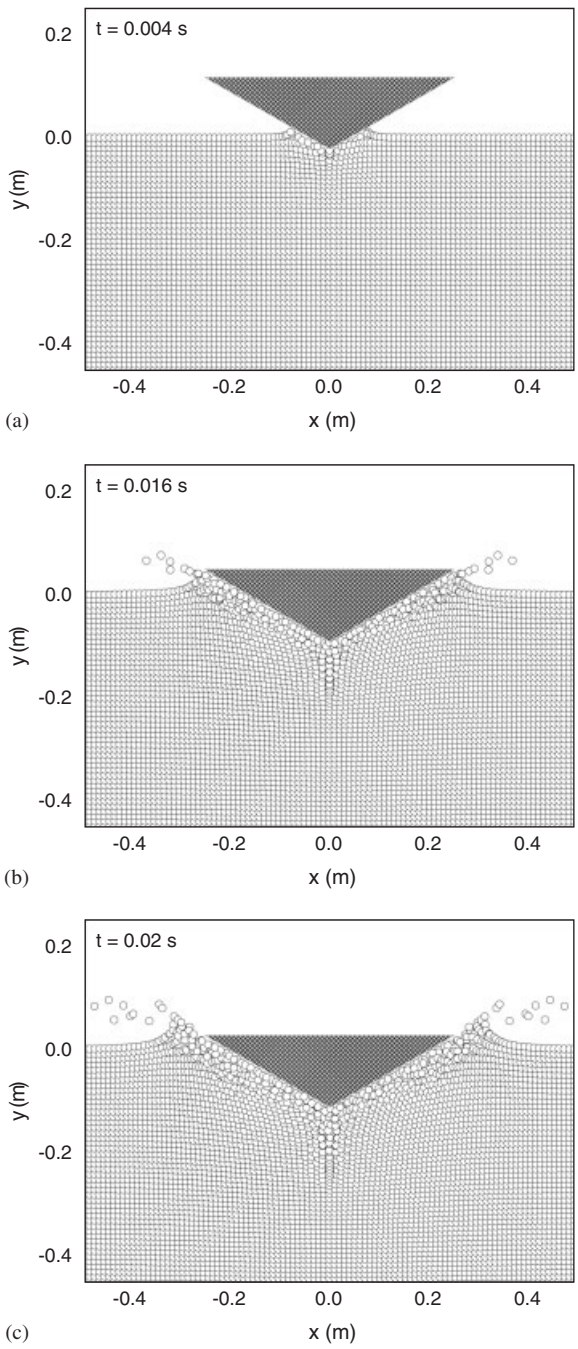

Figure A2. (a)–(c) Particle snapshots without turbulence modeling.

DOI: 10.1002/fld

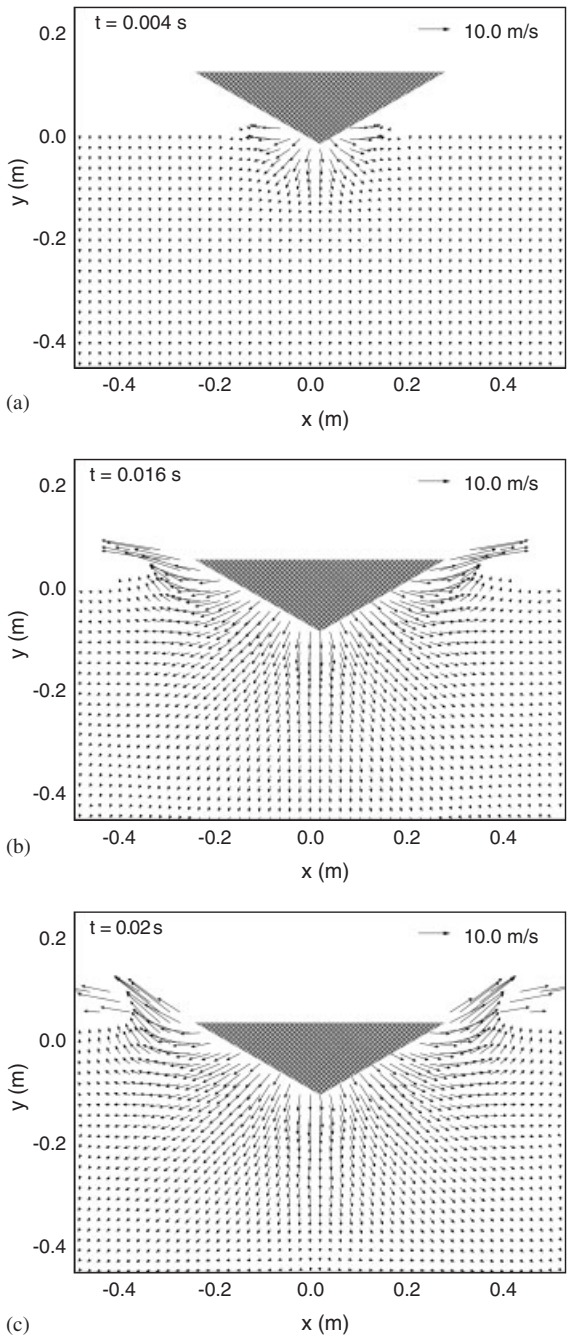

Figure A3. (a)–(c) Velocity fields without turbulence modeling.

DOI: 10.1002/fld

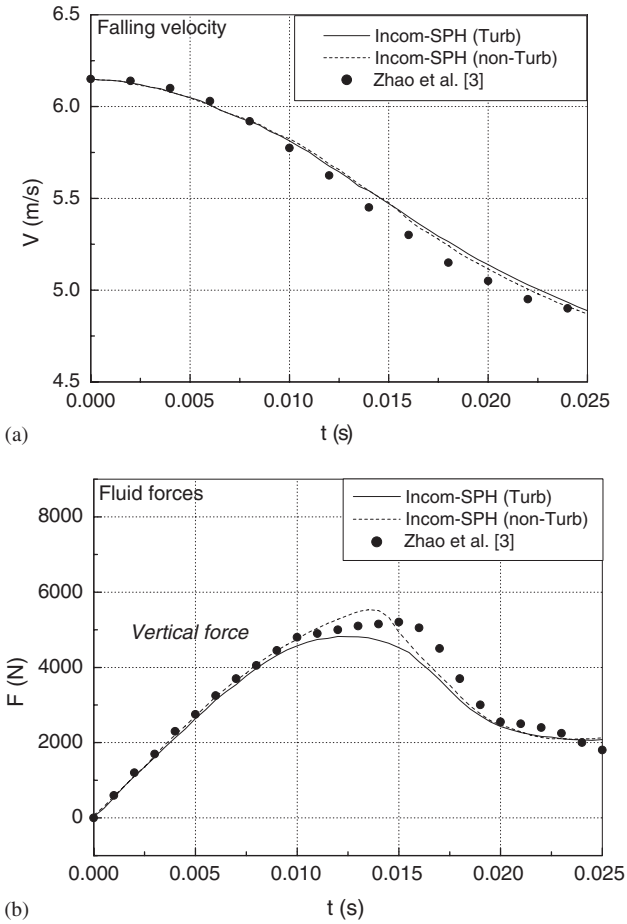

Figure A4. Time history of experimental and computed (a) falling velocity and (b) fluid forces. With both turbulence and non-turbulence results.

of water entry of a circular cylinder. However, Lin [1] cautioned that most potential flow models failed when the impact occurs at the water surface, which was not further addressed in this paper.

NOTATIONS

The following symbols are used in this paper:

a reference particle
b neighboring particle
C_s Smagorinsky constant
F fluid force
$\mathbf{g}$ gravitational acceleration

DOI: 10.1002/fld

h	kernel smoothing distance
I	moment of inertia of solid object
k	turbulence kinetic energy
m	particle mass
n	number of particles constituting solid object
$\mathbf{n}$	normal unit vector on solid boundary
N	number of total particles
P	pressure
P_{mi}	pressure of mirror particles near solid boundary
$\mathbf{q}_k$	relative coordinate of solid particles to solid center
$\mathbf{r}$	position vector
$\mathbf{r}_c$	center of solid object
$\mathbf{r}_k$	position vector of particles constituting solid object
R	particle interaction range in a Verlet table
$\mathbf{R}$	rotational velocity of solid object
$\|S\|$	local strain rate
S_{ij}	element of strain rate
t	time
$\mathbf{t}$	tangential unit vector on solid boundary
$\mathbf{T}$	translational velocity of solid object
$\mathbf{u}$	velocity vector
$\mathbf{u}_k$	velocity vector of particles constituting solid object
$\mathbf{v}_{\mathrm{mi}}$	velocity of mirror particles near solid boundary
$\mathbf{v}_w$	displacement velocity of solid boundary
V	falling velocity of solid object
W	interpolation kernel
x	horizontal coordinate
y	vertical coordinate
δ_{ij}	Kronecker's delta
Δt	time step
ΔX	particle spacing
ε	thickness of Verlet skin
ν_0	laminar viscosity
ν_{T}	turbulence eddy viscosity
ρ	fluid density
ρ_0	initial density
ρ_*	intermediate density
$\overrightarrow{\boldsymbol{\tau}}$	turbulence shear stress
τ_{ij}	element of turbulence stress

ACKNOWLEDGEMENTS

The author is very grateful to Prof. Simon Tait at the University of Bradford, Prof. Hitoshi Gotoh at Kyoto University and Prof. Seiichi Koshizuka at the University of Tokyo for their guidance on the Incom-SPH modeling. The author also acknowledges the support from Prof. Guillaume Oger, Fluid Mechanics Laboratory at Ecole Centrale de Nantes, during the test of the numerical program.

DOI: 10.1002/fld

REFERENCES

1. Lin PZ. A fixed-grid model for simulation of a moving body in free surface flows. *Computers and Fluids* 2007; **36**:549–561.
2. Greenhow M, Lin W. Non-linear free surface effects: experiments and theory. *Report Number 83-19*, Department of Ocean Engineering, Massachusetts Institute of Technology, 1983.
3. Zhao R, Faltinsen O, Aarsnes J. Water entry of arbitrary two-dimensional sections with and without flow separation. *Twenty-first Symposium on Naval Hydrodynamics*, Trondheim, Norway, 1997; 408–423.
4. Tyvand P, Miloh T. Free-surface flow due to impulsive motion of a submerged circular cylinder. *Journal of Fluid Mechanics* 1995; **286**:67–101.
5. Greenhow M, Moyo S. Water entry and exit of horizontal circular cylinders. *Philosophical Transactions of the Royal Society*, *Series A* 1997; **355**:551–563.
6. Kleefsman KMT, Fekken G, Veldman AEP, Iwanowski B, Buchner B. A volume-of-fluid based simulation method for wave impact problems. *Journal of Computational Physics* 2005; **206**:363–393.
7. Panahi R, Jahanbakhsh E, Seif MS. Development of a VoF-fractional step solver for floating body motion simulation. *Applied Ocean Research* 2006; **28**:171–181.
8. Koshizuka S, Nobe A, Oka Y. Numerical analysis of breaking waves using the moving particle semi-implicit method. *International Journal for Numerical Methods in Fluids* 1998; **26**:751–769.
9. Gotoh H, Sakai T. Key issues in the particle method for computation of wave breaking. *Coastal Engineering* 2006; **53**:171–179.
10. Monaghan JJ. Smoothed particle hydrodynamics. *Annual Review of Astronomy and Astrophysics* 1992; **30**: 543–574.
11. Dalrymple RA, Rogers BD. Numerical modeling of water waves with the SPH method. *Coastal Engineering* 2006; **53**:141–147.
12. Oger G, Doring M, Alessandrini B, Ferrant P. Two-dimensional SPH simulations of wedge water entries. *Journal of Computational Physics* 2006; **213**:803–822.
13. Shao SD, Lo EYM. Incompressible SPH method for simulating Newtonian and non-Newtonian flows with a free surface. *Advances in Water Resources* 2003; **26**:787–800.
14. Lee ES, Laurence D, Stansby PK, Violeau D, Moulinec C. 2D flow past a square cylinder in a closed channel. *SPHERIC Newsletter*, *No. 3*, 2006.
15. Shao SD, Ji CM, Graham DI, Reeve DE, James PW, Chadwick AJ. Simulation of wave overtopping by an incompressible SPH model. *Coastal Engineering* 2006; **53**:723–735.
16. Shao SD, Gotoh H. Simulating coupled motion of progressive wave and floating curtain wall by SPH-LES model. *Coastal Engineering Journal* 2004; **46**:171–202.
17. Smagorinsky J. General circulation experiments with the primitive equations, I. The basic experiment. *Monthly Weather Review* 1963; **91**:99–164.
18. Cummins SJ, Rudman M. An SPH projection method. *Journal of Computational Physics* 1999; **152**:584–607.
19. Colagrossi A, Landrini M. Numerical simulation of interfacial flows by smoothed particle hydrodynamics. *Journal of Computational Physics* 2003; **191**:448–475.
20. Viccione G, Bovolin V, Caratelli EP. A fast neighbor-search algorithm for free surface flow simulations using SPH. *ECCOMAS Thematic Conference on Computational Methods in Structural Dynamics and Earthquake Engineering*, Rethymno Crete, Greece, 13–16 June 2007.

DOI: 10.1002/fld